

End-to-End Lidar-Camera Self-Calibration for Autonomous Vehicles

Arya Rachman*[†] Jürgen Seiler* André Kaup*

*Multimedia Communications and Signal Processing
Friedrich-Alexander-Universität Erlangen-Nürnberg
Erlangen, Germany
Email: {firstname.lastname}@fau.de

[†]Product Segment Autonomous Driving
AVL Software and Functions, GmbH
Regensburg, Germany

Abstract—Autonomous vehicles are equipped with a multi-modal sensor setup to enable the car to drive safely. The *initial* calibration of such perception sensors is a highly matured topic and is routinely done in an automated factory environment. However, an intriguing question arises on how to maintain the calibration quality throughout the vehicle’s operating duration. Another challenge is to calibrate multiple sensors jointly to ensure no propagation of systemic errors. In this paper, we propose Camera Lidar Calibration Network (CaLiCaNet), an end-to-end deep self-calibration network which addresses the automatic calibration problem for pinhole camera and Lidar. We jointly predict the camera intrinsic parameters (focal length and distortion) as well as Lidar-Camera extrinsic parameters (rotation and translation), by regressing feature correlation between the camera image and the Lidar point cloud. The network is arranged in a Siamese-twin structure to constrain the network features learning to a mutually shared feature in both point cloud and camera (Lidar-camera constraint). Evaluation using KITTI datasets shows that we achieve 0.154° and 0.059 m accuracy with a reprojection error of 0.028 pixel with a single-pass inference. We also provide an ablative study of how our end-to-end learning architecture offers lower terminal loss (21% decrease in rotation loss) compared to isolated calibration.

Index Terms—self-calibration, Lidar, camera, end-to-end learning, autonomous vehicle, multi-sensor

I. INTRODUCTION

Modern vehicles are equipped with multi-modal sensors, enabling perception algorithms to better understand the environment. Compared to classical camera-only perception, adding depth-capable sensors such as Radar and Lidar enables unambiguous recognition in a 3D world. Therefore, a camera and Lidar combination is the most used in autonomous vehicle setup, often with multiple instances of the same modality (e.g., $2 \times$ Lidar plus $3 \times$ camera).

The use of such multi-sensor setups comes with the need for cascaded calibration: first, each sensor needs to be both calibrated intrinsically relative to its internals, and after that, it needs to be extrinsically calibrated to other sensors. Both calibrations are prerequisites for sensor fusion, a building block of vehicle perception. In order to perceive the environment consistently, the vehicle has to use sensor measurements in a common coordinate system.

The quality of intrinsic calibration generally impacts extrinsic calibration. Minor errors in the intrinsic calibration may affect the extrinsic calibration’s accuracy. To tackle this problem, jointly-optimized intrinsic and extrinsic calibration is proposed in [1] [2]. The approach offers better performance compared to isolated calibration. However, it requires a static target which is not applicable when a vehicle is in use. For this case, a targetless calibration method is needed.

The classical model-based self-calibration based on Structure-from-Motion (SfM) [3], optical flow [2], and odometry [4] also exist. However, in order to accommodate a broad operating domain and avoid heuristically tuned algorithms, deep-learning-based approaches have been increasingly used for self-calibration (see [5]–[7]). Notwithstanding, the comparison between model-based vs. deep-learning-based approaches remains difficult since there is little-to-no back-to-back comparison, and each approach has a different operating domain, not necessarily automotive. Finally, the deep learning approach primarily relies on supervised networks: this means there is a need for a sufficient amount of labelled, high quality data for the network to properly generalize.

Our previous work [8] introduced a self-calibration pipeline to perform intrinsic camera calibration using deep neural networks and a back-to-back comparison against a target-based method. In this paper, we extend the pipeline with a novel end-to-end learning network called CaLiCaNet, aiming to calibrate a camera intrinsically from scratch and, simultaneously, extrinsically to a Lidar. This is a distinction from the majority of existing Lidar-Camera calibration methods that assume perfect camera intrinsic parameters to be available.

To measure the impact of the proposed architecture, we use evaluation metrics that are directly comparable to conventional pattern-based calibration and benchmark our proposal to a dataset that reflects the target domain: KITTI Datasets [9]. We also include an ablation study treating the intrinsic and extrinsic networks as sub-networks. The aim is to understand how end-to-end networks perform better than isolated networks for Lidar-Camera calibration.

We gratefully acknowledge that this work has been supported by the Bavarian State Ministry of Economic Affairs, Regional Development, and Energy (StMWi) under the EmPer project (grant no. DIK 0179/01).

To summarize, our contributions consist of the following:

- 1) We propose end-to-end CaLiCaNet, which to the best of our knowledge is the first application of end-to-end learning for the purpose of sensor calibration.
- 2) We evaluate our approach using KITTI Dataset with the specific metrics directly comparable to the conventional calibration method. This facilitates an informed decision to switch from the state-of-the-practice to the state-of-the-art calibration approach.
- 3) We propose a streamlined data collection and label generation pipeline for a self-calibrating automotive Lidar-Camera system.

II. RELATED WORKS

Lidar-Camera extrinsic calibration is a well-visited topic. Typically, as a first step, a camera is intrinsically calibrated using a geometric pattern like a checkerboard [10]. Then, its extrinsic calibration to Lidar is done by matching 3D features from the Lidar point cloud to the camera equivalent (i.e., in the image plane). The 3D features from the camera image can be generated from the 3D checkerboard plane or 3D reconstruction method, such as SfM, given the intrinsic parameters.

In practice, the camera intrinsic calibration and Lidar-Camera extrinsic calibration are done (1) sequentially and (2) performed using a specialized pattern before the sensor system is used for intended operation (i.e., offline). Calibrating the camera first, followed by the Lidar-Camera, poses the risk of a systemic error propagating to extrinsic calibration when intrinsic parameters are not sufficiently accurate. Offline calibration also does not consider mechanical shifts occurring during the sensor system operation. The shift is especially relevant for an automotive system, requiring modern vehicles equipped with an array of perception sensors to be periodically recalibrated.

To address the first challenge, we refer to the formulation of joint Lidar-Camera calibration as proposed in [1], [11], [12]. The general idea is to reach a more robust and globally optimal solution bounded by physical measurements of multi-modal sensors. With regard to the second challenge, a global optimization is ideally done without the need for a pattern-like target and uses a natural environment to enable the possibility of online calibration. The SfM-based approach [11] comes close to our needs: natural features are detected using SfM and used as inputs to the Bundle Adjustment algorithm to predict intrinsic parameters. Lastly, Iterative Closest Point (ICP) is used for extrinsic calibration.

Notwithstanding, feature detection and matching using an explicit model require a stable and feature-rich environment and, therefore, generally is not very robust when applied to online calibration. Furthermore, in [11], the evaluation using KITTI dataset is limited to road scenarios (e.g., stable environment), similar limitation can also be found in [3], where it relies on pillar-like structures for the calibration to work. The model-based feature extractor, such as SfM or odometry, typically requires heuristics parameter tuning that

needs to be changed once the operating domain (e.g., camera type or environment) is shifted.

Acknowledging these general difficulties, deep-learning-based perception sensor calibration is proposed, as seen in [5]–[7]. The main idea is to leverage well-validated and pre-trained image detectors (e.g., ImageNet, Inception, ResNet), which are conventionally used for image classification and object detection, as an environmental feature extractor.

For automotive purposes, DeepPTZ [7] is able to calibrate vehicle cameras with the extension we provided in [8]. We also consider LCCNet [6] and CFNet [13], which evaluate their method directly on KITTI Dataset for Lidar-Camera calibration. Still, these deep-learning approaches have yet to address the need to jointly calibrate camera intrinsic and camera extrinsic.

Unlike the classical model-based online calibration, we believe there is no learning-based solution yet that performs Lidar-Camera calibration end-to-end, the implicit assumption being that perfect camera intrinsic is always available and always rigid notwithstanding with a vehicle dynamics (e.g., vibration) influencing sensor and outdoor environment (e.g., temperature) affecting sensor mechanical setup.

Finally, to the best of our knowledge, end-to-end learnings were widely investigated, albeit within a limited domain (e.g., self-driving [14] or text recognition [15]). Therefore, the behaviour of end-to-end network design is only little visited in the field of vehicle perception, especially sensor calibration.

III. SELF-CALIBRATION PROBLEM

A. Problem Formulation

For the camera, we consider the pinhole model following [16], by which lens distortion is modelled using the Unified Spherical Model (USM). The camera intrinsic calibration is formulated as recovering intrinsic parameters K_i , and distortion coefficient ξ_i from i input images.

Meanwhile, the Lidar extrinsic calibration is described by a rigid 3D transform consisting of rotation R_i and translation t_i . For each image i and point cloud $(X, Y, Z)_i$, a point in the 3D world can be projected using matrix K to camera pixel coordinate (u, v) , assuming an undistorted image and no scaling is needed:

$$\begin{bmatrix} u \\ v \\ 1 \end{bmatrix} = K[Rt] \begin{bmatrix} X \\ Y \\ Z \\ 1 \end{bmatrix} \quad (1)$$

When the intrinsic camera parameters and Lidar-Camera parameters estimation are treated within a unified optimization problem, we get a better chance of coming to a globally optimal solution [17]. The advantage is especially relevant since joint optimization provides the physical constraints recognized by both Lidar and the camera.

Based on the above formulation, we delineate our goal of end-to-end Lidar-Camera self-calibration to the acquisition of calibration values $\theta = \{f, \xi, R, t\}$ given sets of image and 3D point cloud pair from natural scenes. The image sensor

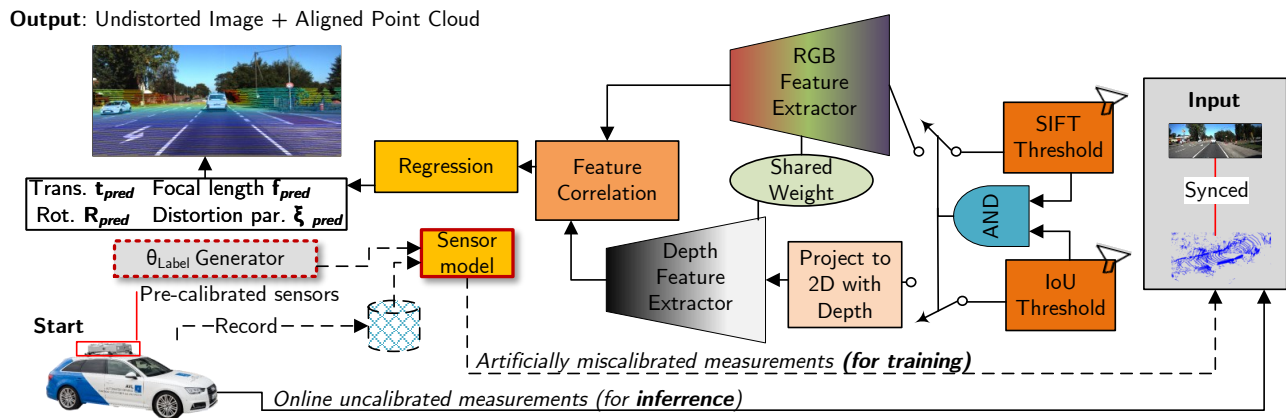


Fig. 1. End-to-end Lidar-Camera Self-Calibration Pipeline with CaLiCaNet. The parts denoted by the dashed line are only used during network training.

is assumed to be square (focal length f is symmetrical along the x - and y -axis), and the Lidar scan is assumed to be ego-motion-compensated. The constraint is that the measurement does not need to have an explicit geometric pattern nor be taken in a specific environment with certain structure features (e.g., pole or building). Considering the difficulty of modelling such an environment, we defer to a learning-based approach.

B. Deep Learning by Driving: Generating Training Data

Deep learning approaches for sensor calibration are largely supervised and thus require labelled ground truth. We refer to the learning-by-driving label generation strategy previously proposed in [8]. Our training label generation strategy does not need human annotation nor additional infrastructure not already existing in a modern car and automotive supply chain. First, we pre-calibrate a pair of camera and Lidar sensor with a checkerboard-based, controlled environment setup to get θ_0 . We consider θ_0 as ground truth calibration values. We then collect the sensor measurements while the car is driving with the target calibration sensors.

The resulting measurements become a dataset of time-series calibrated frames (point cloud and image). Analogous to augmentation, *realistic* (i.e., based on known calibration deviation over a long-term driving period) θ_{label} are generated together along with sets of distorted images and miscalibrated point clouds, as seen in Fig. 1.

IV. END-TO-END DESIGN

A. Isolated Networks

In this work, we adopt networks with public reference implementation as benchmarks and inspirations for our end-to-end design. Following (1), the output of an intrinsic calibration network can be chained directly to an extrinsic calibration network. In this case, the prediction and training of each intrinsic and extrinsic network happen in isolation.

For the intrinsic networks, we adopt some part of DSNet [7], a Siamese-network designed to predict camera intrinsics calibration f and ξ with inputs of two correlated images from different viewpoints. It was originally designed to work

with panoptic datasets and panning, rotation, and zoom (PTZ) camera, but we have extended it in [8] to work with vehicle cameras as the target domain. As for extrinsic calibration, inspired by LCCNet [6], we use a volume-cost-based network that correlates the volume cost shared by the image and the projected point cloud depth image. Both isolated networks rely on features correlation to regress θ .

B. CalicaNet

CaLiCaNet (Camera Lidar Calibration Network) aims to enable effective end-to-end learning by building upon feature extraction networks to associate features from two correlated sensor measurements and regress them into calibration parameters.

Recall that the DSNet feature map is extracted based on two-correlated monocular images to enforce a bi-directionality constraint. While this has been shown to help the network to focus on relevant features, the features from monocular cameras are inherently two-dimensional. Making the network susceptible to the famous "Wile E. Coyote's tunnel" (a tunnel imagery being painted on a wall to induce illusion of depth). We address the problem by enforcing the constraint from two different sensor modalities: Lidar and camera. Compared to a single modality approach, environmental attenuations specific to a camera (e.g., low light or fake depth) are mitigated by a Lidar, and vice versa (e.g., dark object or sparsity).

On the other hand, LCCNet relies on the assumption that the input image is perfectly undistorted and that the camera intrinsic matrix \mathbf{K} is sufficiently accurate. If the lens undistortion is inaccurate, for example, the Lidar-Camera extrinsic prediction can be overfitted to the centre region of the image. More importantly, LCCNet requires multi-pass inferences to achieve sufficient accuracy for autonomous driving. With our CaLiCaNet, we mitigate this problem by explicitly incorporating intrinsic parameters in the loss function and implementing the Lidar-Camera constraint by means of weight sharing. Further details of CaLiCaNet can be found in Fig. 1 as well as in the following subsections:

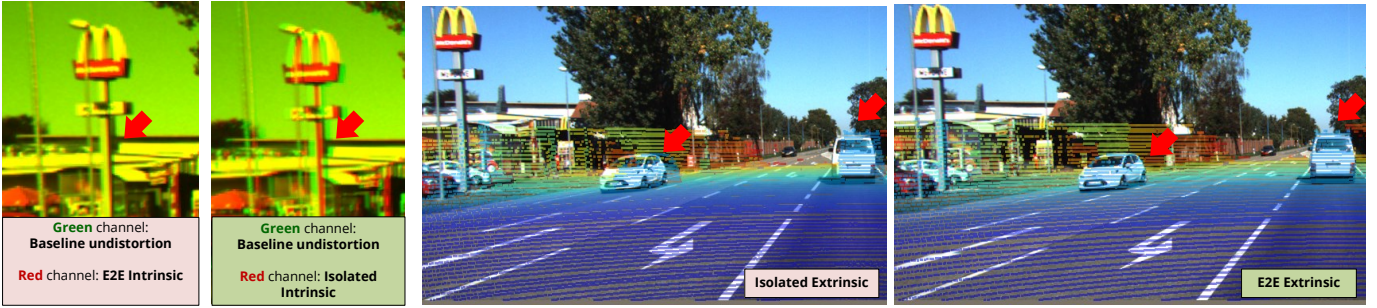


Fig. 2. End-to-End vs Isolated Self-Calibration. **Intrinsic**: red/green halos indicate pixel-wise differences. **Extrinsic**: projected point cloud to an image representing alignment quality. Red arrows point to misalignment regions of interest.

1) **Pre-processing: ensuring consistent input**: We discard featureless images (e.g., frames dominated by sky and rural, empty road) by computing SIFT descriptors on each frame and passing only frames with a certain threshold of key-points count (see [18] for details). Additionally, we also ensure the overlap with the Intersection of Union (IoU) of ≥ 0.5 between an RGB image and the corresponding Lidar 2D projection. These measures are intended so that the network sees more consistent input during training and inference.

2) **Network Architecture**: We use ResNet50 [19] as a feature extractor and implement the necessary fully connected layers for generating the correlation between inputs. Since we aim to use single-pass inference from natural scenes, we choose a deeper network block. In contrast, DSNet uses Inceptionv3, and LCCNet uses ResNet18. We also aim to accept an arbitrary resolution on the training images and point cloud, owing to the diversity of vehicle sensors; therefore, we place an adaptive average pooling before the fully connected layer. Furthermore, we extend the volume-cost-based correlation module from [6] to work with a Siamese structure. Finally, we opt to use Parametrized ReLU (PReLU) for our network extractor activation function. The ReLU weight, therefore, becomes a trainable parameter. Our functional network architecture as part of the end-to-end pipeline is described in Fig. 1.

3) **Loss Functions**: The network minimizes the L2-smooth loss L between regressed calibration values of θ_{pred} and that of label θ_{label} . Except for \mathbf{R} that is converted to equivalent quaternion representation \mathbf{q} , and therefore quaternion distance is treated as a loss. For vehicle perception purposes, the misalignment in translation does not affect vehicle perception as much as rotation (refer to Fig. 2 for an example of misalignment due to rotation). Therefore, we penalize the network more for predicting the wrong rotation. The training loss L_T thus becomes:

$$L_T = \lambda_f L_f + \lambda_\xi L_\xi + \lambda_q L_q + \lambda_t L_t \quad (2)$$

with $\lambda_q \geq \lambda_t$

V. EVALUATION

We propose two evaluation strategies: the first is evaluating with KITTI Dataset to check the performance in a realistic

situation. This serves as validation of our approach. The second strategy is an ablation study to examine closer how an end-to-end architecture enhances the network performance; this serves as verification of our network design. Such two-step approach is a necessary first step in developing safety-critical software running on a vehicle [20].

A. Experimental Setup

1) **Dataset**: To evaluate the calibration accuracy, we use the KITTI Dataset [9], in which the RGB images captured by the right-side monocular camera are used. Ground-truth calibration values θ_0 from the KITTI dataset are generated as follows: we use the OpenCV Omnidirectional Calibration library [21] to perform intrinsic calibration for each daily drive using the corresponding checkerboard recordings. Following the models stated in Section III-A, we obtain θ_0 and the corresponding baseline reprojection root mean square (RMS) error ϵ_0 [16].

2) **Label Generation and Training**: The first day of the KITTI drive (2011-09-26) is used as training labels, while the remaining four days are used for evaluation. We generated the labels by setting the labels' value to θ_0 plus a variable deviation (i.e., the miscalibration). The label generation refers to physical changes on the sensors induced by mechanical and environmental factors during everyday driving and is set to $\theta_{label} = \{f \pm 100\text{px}, \xi \pm 0.48, \mathbf{R} \pm 2.0^\circ, \mathbf{t} \pm 0.2\text{m}\}$. The distorted image and misaligned point cloud pairs are generated according to θ_0 . In total, we generated approximately 120 000 labels (θ_{label} , image and point cloud) split into 80:20 ratios for training and validation datasets. Adam Optimizer is used with an initial learning rate of 3×10^{-3} . The batch size used was 60 with maximum epochs of 300.

3) **Evaluation Metrics**: For calculating the intrinsic calibration accuracy, we use KITTI's checkerboard which contain i corners $\{p_{1j}, p_{2j}, \dots, p_{ij}\} \in \mathbb{R}^3$ from j -th checkerboard poses \mathbf{Rt} . The purpose is to calculate the Root Mean Squared Error (RMSE) of the reprojection ϵ in pixels, given as:

$$\epsilon = \sqrt{\frac{1}{N} \sum_{i=1} \sum_{j=1} \|\mathbf{K}[\mathbf{Rt}]p_{ij} - x_{ij}\|_2} \quad (3)$$

Note that this reprojection error value obtained based on θ_0 is considered as the *baseline* reprojection error ϵ_0 . When our

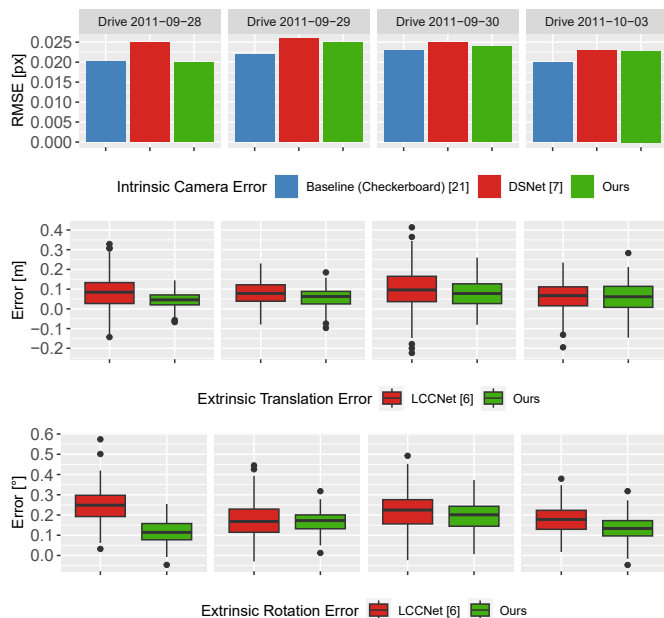


Fig. 3. Intrinsic and extrinsic calibration error. For intrinsic, the baseline is the best achievable RMS reprojection error obtained with the checkerboard-based calibration. For extrinsic, we calculate the mean error of all 3D axes. DSNet [7] and LCCNet [6] were trained isolated and only single pass inference was used. See Fig. 2 for the accompanying visualization and Table I for mean values across all drives.

network infers θ_{pred} , the detected corners and checkerboard poses are reused to calculate inference reprojection error ϵ_{pred} . We consider ϵ_{pred} to be more representative of calibration quality relative to the comparison of the intrinsic part of θ_0 to θ_{pred} . We refer to [16] for more in-depth reasoning.

On the other hand, for extrinsic calibration, for the sake of comparability, we opt to follow the convention in prior works [6], [11], [22] by directly comparing the extrinsic part of θ_0 to that of θ_{pred} , that is the mean error of rotation and translation. In this case, the baseline extrinsic error is assumed to be zero.

B. KITTI Drives

The evaluation using KITTI drives is intended to show CaLiCaNet accuracy and robustness when applied to diverse driving scenarios. Referring to Fig. 3, the mean error below 0.028 px across all four days of driving shows that our approach is comparable to classical checkerboard-based intrinsic calibration in terms of reprojection error. The significance of this low error can be visually inspected in Fig. 2. When the DSNet network is trained in isolation, we noted an error increase of almost 20% relative to our proposed end-to-end approach (see drive 2011-09-28 in Fig. 3). Additionally, the undistortion result in Fig. 2 (second image from the left) corroborates the increased error. Up to 15 pixels differences can be seen on the edge region of the image, where the distortion effect is more present.

A similar effect can be found in the extrinsic calibration: the end-to-end approach results in better Lidar-Camera alignment. Due to the intended use of online calibration, we put a

TABLE I
AVERAGE INTRINSIC AND EXTRINSIC CALIBRATION ERRORS

Calibration Error	Baseline [21]	DSNet [7]	LCCNet [6]	Ours
Intrinsic [px]	0.018	0.024	-	0.021
Extrinsic \mathbf{t} [m]	-	-	0.082	0.060
Extrinsic \mathbf{R} [°]	-	-	0.204	0.154

TABLE II
ABLATION STUDY EXPERIMENTS

Exp.	RGB train?	Depth train?	Siamese?	f -loss	ξ -loss	\mathbf{R} -loss	\mathbf{t} -loss
I	\times	\checkmark	\times	-	-	6.658E-4	0.0014
II	\checkmark	\times	\times	11.41	0.070	-	-
III	\checkmark	\checkmark	\times	11.41	0.068	6.054E-4	0.0010
IV	\checkmark	\checkmark	\checkmark	11.02	0.067	4.758E-4	0.0010

constraint that the inference must happen in a single pass (no iteration). Under this constraint, we achieve a noticeably better mean rotational accuracy compared to when the LCCNet is trained in isolation (0.154° vs. 0.203°).

We can infer some robustness by inspecting the statistical fluctuation of CaLiCaNet prediction in Fig. 3. Across four days of driving with notably diverse sceneries (city, campus, residential, and road, see [9] for more details) the maximum intrinsic and extrinsic calibration errors remain below 0.028 px and 0.4°/0.2m, respectively. For extrinsic error, our outlier values are decisively lower than that of LCCNet, which we attribute to the Lidar-Camera measurement constraint realized by the weight sharing. Notwithstanding, we note the lowered accuracy in drive 2011-10-03 and bigger spread since the drive is dominated by highway sceneries (i.e., fewer edge and line-like features to extract). With this finding, we consider it beneficial if the car drives in a feature-rich environment (e.g., inner city) when the self-calibration functionality is active.

Overall, we consider the KITTI Drives evaluation result to appropriately reflect CaLiCaNet fitness for vehicle sensors self-calibration. It fulfils its purpose of avoiding a miscalibration, as illustrated in Fig. 2; which can and will compromise the road object localization capability of a road vehicle.

C. Ablation Study

We conducted ablation studies to evaluate the influence of end-to-end training on Lidar-Camera accuracy. Essentially, this study attempts to pinpoint which part of the pipeline is responsible for the improved performance. The evaluation metrics used are the validation terminal loss.

We used the identical setup in Section V-A, but varied our training strategy and the corresponding network architecture. First, the feature extractors are no longer sharing weights. In experiment I, we froze the layers of the RGB extractor before training the network. In experiment II, we froze the layers of the depth extractor instead. In experiment III, all layers of the feature extractors are trainable, but the weight sharing is not activated. Finally, in Experiment IV, the normal end-to-end training with Siamese weight sharing was performed. The results can be seen in Table II.

It is quite evident that end-to-end training results in lower losses overall. The extrinsic parameters regressor (especially rotation with a decrease of 21%) benefits the most when trained in both end-to-end and Siamese configurations (see **R**-loss and **t**-loss). However, we have observed that intrinsic calibration losses (f -loss and ξ -loss) do not appear to have a significant effect when trained end-to-end (loss decrease of less than 1%). However, when the weight sharing is activated, we see a modest decrease in intrinsic losses (3%). This may suggest that the feature-extracting networks cannot properly generalize the relevant feature for camera intrinsic parameters.

The behaviour of the intrinsic calibration network can be potentially explained by insufficient edge coverage from the KITTI checkerboard recording. The distortion on the far-edge region of the image is not fully modelled and may result in suboptimal baseline calibration θ_0 , and by extension, θ_{label} . In addition, the USM model used does not consider the tangential and radial distortion [23]. Based on this study, we learned the limitation of our label generation strategy, which heavily relies on good checkerboard recording. For real applications and future works, the training label should be based on a checkerboard recording of sufficient coverage and tangential and distortion models should be considered.

VI. CONCLUSION

We have proposed a novel end-to-end learning strategy for jointly self-calibrating camera and Lidar sensor with the accompanying deep neural network CaLiCaNet. The pipeline proposed a label generation strategy with a normally operating vehicle and existing calibration infrastructure. It also ensures the quality of the inputs to the self-calibration pipeline by means of detecting SIFT key-points and detecting Lidar-Camera measurements overlap. Our main contribution lies in the design of CaLiCaNet, consisting of two feature extractor networks (one for camera image and one for Lidar point cloud) arranged in a Siamese structure. The design is devised to deal with the limitation of using single sensor modality (i.e., bottlenecked by a single sensor physical limitation) and mitigating the propagation of error when estimating extrinsic calibration using unverified intrinsic calibration.

Finally, we performed thorough verification and validation based on an ablation study and evaluation with realistic driving scenarios. Our approach is shown to perform well when compared to classical, infrastructure-bounded checkerboard calibration. Furthermore, compared to other learning-based approaches, our approach can outperform isolated intrinsic and extrinsic self-calibration with a single-pass inference, paving its way to adoption in real-world online applications.

REFERENCES

- [1] M. Hillemann and B. Jutzi, "UCalMiCeL – Unified Intrinsic and Extrinsic Calibration of a multi-Camera-System and a Laserscanner," *ISPRS Ann. Photogramm. Remote Sens. Spat. Inf. Sci.*, vol. IV-2/W3, no. 2W3, pp. 17–24, Aug. 2017.
- [2] A. Kodaira, Y. Zhou, P. Zang, W. Zhan, and M. Tomizuka, "SST-Calib: Simultaneous Spatial-Temporal Parameter Calibration between LIDAR and Camera," in *2022 IEEE 25th Int. Conf. Intell. Transp. Syst.*, Oct. 2022, pp. 2896–2902.

- [3] B. Nagy and C. Benedek, "On-the-Fly Camera and Lidar Calibration," *Remote Sens.*, vol. 12, no. 7, p. 1137, Apr. 2020.
- [4] L. Heng, Bo Li, and M. Pollefeys, "CamOdoCal: Automatic intrinsic and extrinsic calibration of a rig with multiple generic cameras and odometry," in *2013 IEEE/RSJ Int. Conf. Intell. Robot. Syst.*, Nov. 2013, pp. 1793–1800.
- [5] O. Bogdan, V. Eckstein, F. Rameau, and J.-C. Bazin, "DeepCalib," in *Proc. 15th ACM SIGGRAPH Eur. Conf. Vis. Media Prod.*, no. December. New York, NY, USA: ACM, Dec. 2018, pp. 1–10.
- [6] X. Lv, B. Wang, Z. Dou, D. Ye, and S. Wang, "LCCNet: LiDAR and Camera Self-Calibration using Cost Volume Network," in *2021 IEEE/CVF Conf. Comput. Vis. Pattern Recognit. Work.*, Jun. 2021, pp. 2888–2895.
- [7] C. Zhang, F. Rameau, J. Kim, D. M. Argaw, J.-C. Bazin, and I. S. Kweon, "DeepPTZ: Deep Self-Calibration for PTZ Cameras," in *2020 IEEE Winter Conf. Appl. Comput. Vis.*, Mar. 2020, pp. 1030–1038.
- [8] A. Rachman, J. Seiler, and A. Kaup, "Camera Self-Calibration: Deep Learning from Driving Scenes," in *2022 IEEE Int. Conf. Image Process.*, Oct. 2022, pp. 2836–2840.
- [9] A. Geiger, P. Lenz, C. Stiller, and R. Urtasun, "Vision meets robotics: The KITTI dataset," *Int. J. Rob. Res.*, vol. 32, no. 11, pp. 1231–1237, Sep. 2013.
- [10] Z. Zhang, "A flexible new technique for camera calibration," *IEEE Trans. Pattern Anal. Mach. Intell.*, vol. 22, no. 11, pp. 1330–1334, 2000.
- [11] D. Tu, B. Wang, H. Cui, Y. Liu, and S. Shen, "Multi-Camera-LiDAR Auto-Calibration by Joint Structure-from-Motion," in *2022 IEEE/RSJ Int. Conf. Intell. Robot. Syst.*, vol. 2022-October, Oct. 2022, pp. 2242–2249.
- [12] J. Ou, P. Huang, J. Zhou, Y. Zhao, and L. Lin, "Automatic Extrinsic Calibration of 3D LIDAR and Multi-Cameras Based on Graph Optimization," *Sensors*, vol. 22, no. 6, p. 2221, Mar. 2022.
- [13] X. Lv, S. Wang, and D. Ye, "CFNet: LiDAR-Camera Registration Using Calibration Flow Network," *Sensors*, vol. 21, no. 23, p. 8112, Dec. 2021.
- [14] A. Tampuu, T. Matiisen, M. Semikin, D. Fishman, and N. Muhammad, "A Survey of End-to-End Driving: Architectures and Training Methods," *IEEE Trans. Neural Networks Learn. Syst.*, vol. 33, no. 4, pp. 1364–1384, Apr. 2022.
- [15] B. Shi, X. Bai, and C. Yao, "An End-to-End Trainable Neural Network for Image-Based Sequence Recognition and Its Application to Scene Text Recognition," *IEEE Trans. Pattern Anal. Mach. Intell.*, vol. 39, no. 11, pp. 2298–2304, Nov. 2017.
- [16] R. Hartley and A. Zisserman, *Multiple View Geometry in Computer Vision*, 2nd ed. New York, NY, USA: Cambridge University Press, 2003.
- [17] G. Yan, F. He, C. Shi, X. Cai, and Y. Li, "Joint Camera Intrinsic and LiDAR-Camera Extrinsic Calibration," Feb. 2022.
- [18] D. G. Lowe, "Distinctive Image Features from Scale-Invariant Key-points," *Int. J. Comput. Vis.*, vol. 60, no. 2, pp. 91–110, Nov. 2004.
- [19] K. He, X. Zhang, S. Ren, and J. Sun, "Deep Residual Learning for Image Recognition," in *2016 IEEE Conf. Comput. Vis. Pattern Recognit.*, vol. 2016-December, Jun. 2016, pp. 770–778.
- [20] J. Zhang and J. Li, "Testing and verification of neural-network-based safety-critical control software: A systematic literature review," *Inf. Softw. Technol.*, vol. 123, no. March, p. 106296, Jul. 2020.
- [21] G. Bradski, "OpenCV Library," *Dr. Dobb's J. Softw. Tools*.
- [22] A. D. Nguyen and M. Yoo, "CalibBD: Extrinsic Calibration of the LiDAR and Camera Using a Bidirectional Neural Network," *IEEE Access*, vol. 10, no. September, pp. 121 261–121 271, 2022.
- [23] C. Mei and P. Rives, "Single View Point Omnidirectional Camera Calibration from Planar Grids," in *Proc. 2007 IEEE Int. Conf. Robot. Autom.*, Apr. 2007, pp. 3945–3950.